An Adaptive Groundtrack Maintenance Scheme for Spacecraft with Electric Propulsion

Mirko Leomanni[1], Andrea Garulli, Antonio Giannitrapani

Dipartimento di Ingegneria dell'Informazione e Scienze Matematiche
Università di Siena, Siena, Italy

Fabrizio Scortecci

Aerospazio Tenologie
Rapolano Terme, Siena, Italy

Abstract

In this paper, the repeat-groundtrack orbit maintenance problem is addressed for spacecraft driven by electric propulsion. An adaptive solution is proposed, which combines an hysteresis controller and a recursive least squares filter. The controller provides a pulse-width modulated command to the thruster, in compliance with the peculiarities of the electric propulsion technology. The filter takes care of estimating a set of environmental disturbance parameters, from inertial position and velocity measurements. The resulting control scheme is able to compensate for the groundtrack drift due to atmospheric drag, in a fully autonomous manner. A numerical study of a low Earth orbit mission confirms the effectiveness of the proposed method.

Keywords: Ground Track Maintenance, Electric Propulsion, Low Earth Orbit

1. Introduction

Recent years have seen a growing trend in the development of Low Earth Orbit (LEO) space missions for commercial, strategic, and scientific purposes. Examples include Earth Observation programs such as DMC, RapidEye and Pléiades-Neo [1, 2], as well as broadband constellations like OneWeb, Starlink

Email addresses: leomanni@diism.unisi.it (Mirko Leomanni), garulli@diism.unisi.it (Andrea Garulli), giannitrapani@diism.unisi.it (Antonio Giannitrapani), fscortecci@aerospazio.com (Fabrizio Scortecci)
[1]Corresponding author

and Telesat [3]. As opposed to geostationary spacecraft, a LEO satellite cannot stay always pointed towards a fixed spot on Earth. Nevertheless, it can revisit the same location periodically, by using a repeat-groundtrack orbit configuration. Besides its utility in traditional remote sensing applications, such a configuration can be exploited to deploy satellite constellations supporting global, regional and reconnaissance services [4, 5]. Thus, a repeat-groundtrack orbit design is ubiquitous in the above-mentioned type of missions.

Due to environmental perturbations and, in particular, to atmospheric drag, the groundtrack of a LEO satellite tends to drift away from the nominal repeat condition. This undesired effect must be compensated for by means of a suitable groundtrack maintenance program. Depending on the required control accuracy, the program may involve a tight maneuvering schedule, which makes ground-based control inefficient and risky. In order to overcome this issue, a variety of autonomous on-board control strategies have been proposed, see e.g., [6, 7, 8, 9].

Groundtrack maintenance operations require an adequately sized propulsion unit. The unit must produce the delta-v associated to the maintenance program, in addition to the one reserved for orbit acquisition and de-orbiting maneuvers. The latter, in particular, are mandatory within present regulations [10]. For very low altitude orbits, drag compensation can be the dominant factor in the mission delta-v budget, while the contribution due to de-orbiting becomes more pronounced at higher altitudes. In any case, the total delta-v may grow to a level justifying the adoption of a high specific impulse, low-thrust technology such as Electric Propulsion (EP) [11, 12, 13, 14]. Indeed, a number of EP-based LEO missions have been recently launched [15].

The maintenance of repeat-groundtrack orbits is a well-established topic in astrodynamics. The classical open-loop solution to the maintenance problem is described, for instance, in [16]. Several modifications to this method have been proposed in the literature. In [17], a feedback implementation is presented. The effect of a moderate orbital eccentricity is analyzed in [18]. The application to successive-coverage orbits is discussed in [19]. A high-precision design is presented in [20]. In all these works, each engine burn is modeled as an impulsive velocity change. Such an approximation is not well suited for EP engines, whose thrust profile is usually modeled as a rectangular pulse. In light of this consid-

eration, some recent studies [21, 22] have started adopting a piecewise-constant parametrization of the control command.

In this paper, an autonomous groundtrack maintenance strategy is developed for EP-based LEO missions. In compliance with the peculiarities of the EP technology, it is assumed that the thruster is either operated at a constant set-point or switched off, thus requiring a pulse-width modulated control input signal. It is shown that, for small deviations about a circular orbit, the groundtrack error dynamics is that of a perturbed double integrator. The perturbation term is modeled as a periodic signal with non-zero mean, according to what is observed in the literature [16]. Within this setting, an adaptive feedback scheme is derived. The idea underpinning the design is to combine an hysteresis controller with a recursive least squares (RLS) filter. The RLS filter is in charge of estimating a set of parameters of the error system. The controller provides a suitable on/off engine switching signal based on the filter estimates. The control law builds upon recent results on minimum switching control in [23, 24]. Although both RLS estimation and switching control are well established methodologies, the main contribution of this work is to suitably adapt these techniques to the specific application of repeat-groundtrack orbit maintenance.

The proposed control scheme is evaluated on a simulation case study featuring a 460 km altitude orbit. Simulation results show that the desired repeat-groundtrack pattern is acquired successfully and that the tracking error is maintained within prescribed limits, relying only on GPS measurements.

The rest of the paper is organized as follows. In Section 2, the repeat-groundtrack control problem is reviewed. Section 3 presents the dynamic model which is employed for control design. The adaptive groundtrack control scheme is described in Section 4. The simulation case study is discussed in Section 5, and conclusions are drawn in Section 6.

2. Problem Formulation

Repeat-groundtrack orbits depend on the commensurability between the satellite nodal period (the time interval it takes a satellite to make two consecutive ascending node crossings), and the nodal period of Greenwich (the

period of the Earth's rotation with respect to the ascending node). The nodal period is defined as

$$T_\gamma = \frac{2\pi}{\dot{\gamma}}, \tag{1}$$

where $\gamma = M + \omega$ is the satellite mean latitude, i.e., the sum of the mean anomaly M and of the argument of periapsis ω. The nodal period of Greenwich is given by

$$T_G = \frac{2\pi}{\omega_\oplus - \dot{\Omega}}, \tag{2}$$

where $\omega_\oplus$ is the Earth's rotation rate, and Ω is the satellite right ascension of the ascending node. Thus, the repeat-groundtrack condition can be formalized as

$$T_\gamma = r\, T_G, \tag{3}$$

where $r > 0$ is a rational number, representing the ratio between the number of days and the number of satellite revolutions within the repeat cycle. For LEO orbits, r is typically in the order of $1/15$.

The groundtrack spacing λ_S between two consecutive ascending node crossings is given by

$$\lambda_S = 2\pi \frac{T_\gamma}{T_G}. \tag{4}$$

Ideally, $\lambda_S = 2\pi r$. However, in the presence of perturbations such as atmospheric drag and third-body gravity, λ_S drifts away from the nominal value. In standard repeat-groundtrack control schemes, a sequence of impulsive orbit adjustment maneuvers is commanded to counteract this change [16]. In this paper, a different approach is proposed.

Besides enforcing (3), the control scheme must guarantee that the satellite repeatedly crosses the equator at a desired longitude $\lambda^* \in [0, 2\pi)$, east of Greenwich. Let $\lambda_G(t) = \lambda_G(0) + \omega_\oplus t$ be the instantaneous longitude of Greenwich. Then, the groundtrack error $x(t)$ is defined as

$$x(t) := r\,\gamma(t) + \Omega(t) - \lambda_G(t) - \lambda^*, \tag{5}$$

where all angular quantities are unwrapped. Notice that when $x(t)$ is constant, i.e. $\dot{x}(t) = 0$, one has

$$r\,\dot{\gamma} + \dot{\Omega} - \omega_\oplus = 0, \tag{6}$$

which in turn, by using (1) and (2), implies that (3) is satisfied. Moreover, if $x(t) = 0$, then the satellite crosses the equator at the desired east longitude λ^*. In fact, by definition $\gamma = 2\pi N$, with $N \in \mathbb{N}$, whenever the satellite crosses the ascending node. Being r in (3) a rational number, there exists an ascending node crossing time t_c, at which

$$[r\,\gamma(t_c)] \mod 2\pi = 0. \tag{7}$$

By using (7) and $x(t) = 0$, it follows from (5) that

$$[\Omega(t_c) - \lambda_G(t_c)] \bmod 2\pi = \lambda^*, \tag{8}$$

where the expression on the left hand side is indeed the satellite east longitude at the equator crossing time t_c.

The requirement $x(t) = 0$, $\forall t$, cannot be achieved with a on/off thrusting strategy. Therefore, the following relaxed control problem is addressed.

Problem 1. *Find an on/off thrusting scheme, ensuring that*

$$|x(t)| \leq x_{lim} \quad \textit{for all } t \geq \tilde{t} > 0, \tag{9}$$

where $x_{lim} > 0$ is a predefined longitude error tolerance, and $\tilde{t}$ is a finite settling time.

Following a common practice, we consider tangential thrust only. In fact, radial and out-of-plane maneuvers are often deemed too expensive in terms of fuel consumption [16]. In this regard, it should be noticed that Problem 1 does not account for the grountrack deviation resulting from inclination errors (which is zero at the equator and increases with the latitude). Such contribution can be compensated for separately, if required, via out-of-plane maneuvers. Moreover, attention is restricted to the case of a near-circular orbit, since most LEO spacecraft are flown in this type of orbit.

3. Groundtrack Error Dynamics

The dynamics of the groundtrack error are obtained by taking the second derivative of (5) with respect to time, resulting in

$$\ddot{x}(t) = r\,\ddot{\gamma}(t) + \ddot{\Omega}(t). \tag{10}$$

Let the scalar $u_T(t)$ be a tangential control acceleration and the vector $d(t) = [d_R \; d_T \; d_N]^T$ describe the radial, tangential and normal components of a perturbation due to environmental sources. The effect of u_T and d on system (10) can be modeled through the following variational equations, adapted for nearly circular orbits (see, e.g., [7, 25])

$$\begin{aligned} \frac{\mathrm{d}}{\mathrm{dt}}\gamma &= n - \sqrt{\frac{a}{\mu}}\Big[2d_R + \sin(\gamma)\cot(i)\, d_N\Big] \\ \frac{\mathrm{d}}{\mathrm{dt}}n &= -\frac{3}{a}(d_T + u_T) \\ \frac{\mathrm{d}}{\mathrm{dt}}\Omega &= \sqrt{\frac{a}{\mu}}\frac{\sin(\gamma)}{\sin(i)}\, d_N \\ \frac{\mathrm{d}}{\mathrm{dt}}i &= \sqrt{\frac{a}{\mu}}\cos(\gamma)\, d_N, \end{aligned} \tag{11}$$

where the dependence on time is left implicit, $n = \sqrt{\mu/a^3}$ denotes the mean motion, a and i indicate the semi-major axis and inclination, respectively, and μ is the gravitational parameter. By using (11), it can be verified that, for small deviations about an orbit with semi-major axis a^*, (10) takes on the form

$$\ddot{x}(t) = p_d(t) - \frac{3\, r}{a^*}\, u_T(t), \tag{12}$$

where the time varying quantity $p_d(t)$ describes the cumulative effect of environmental perturbations.

Finding an analytical expression for $p_d(t)$ is in general a formidable task. Moreover, such an expression will unavoidably suffer form inaccuracies in the perturbation model adopted for the term $d(t)$. For the problem at hand, it is known that $p_d(t)$ is approximately constant, on average, over few orbital periods [16]. Hence, within such a time scale, $p_d(t)$ can be modeled as

$$p_d(t) = p + p_\Delta(t), \tag{13}$$

where p denotes the average contribution of perturbations, and the term $p_\Delta(t)$ accounts for zero-mean periodic effects.

It is worth noticing that the tangential acceleration due to atmospheric drag usually represents the major contribution to the disturbance component p in (13). More specifically, one has that $p \simeq -3\, r\, \bar{d}_T/a^* > 0$, where $\bar{d}_T < 0$ denotes the average drag acceleration. Conversely, secular perturbations on γ and Ω have a limited impact on (13). For instance, a secular drift of Ω due to the

Sun-synchronicity condition $\dot{\Omega} = 2\pi$ rad/year would result in $\ddot{\Omega} = 0$ in (10), which in turn does not provide any contribution to (13).

4. Repeat-Groundtrack Control Scheme

In this section, an on/off control law is presented for Problem 1, under the assumption that full state information is available and considering an averaged model of the groundtrack error dynamics. Then, a RLS filter is derived, which estimates both the system state and the average disturbance p. Finally, the implementation of an adaptive control scheme based on this modules is discussed, together with a tuning strategy which minimizes the variation of the orbital eccentricity due to thrusting.

4.1. Controller Design

In order to compensate for a constant positive disturbance $p_d(t) = p$ in (12), consider a on/off control input of the form

$$u_T = u_{\max}\, v(t), \tag{14}$$

where $u_{\max} > 0$ is the maximum acceleration which can be delivered by the propulsion system and $v(t) \in \{0, 1\}$ is the engine activation signal. By enforcing (14) and taking into account that $p_\Delta(t)$ is a zero-mean signal, the following averaged model is obtained from (12)-(13)

$$\ddot{y}(t) = p - k\, v(t), \tag{15}$$

where

$$k = \frac{3\, r\, u_{\max}}{a^*}, \tag{16}$$

and $y(t)$ denotes the average groundtrack error.

Let $y(t)$ be the solution to system (15) starting from the initial conditions $y(0) = x(0)$ and $\dot{y}(0) = \dot{x}(0)$. Clearly, the relationship between $y(t)$ and the solution $x(t)$ of system (12) is

$$y(t) = x(t) - \alpha(t), \tag{17}$$

where

$$\alpha(t) = \iint_0^t p_\Delta(\tau)\, \mathrm{d}\tau \tag{18}$$

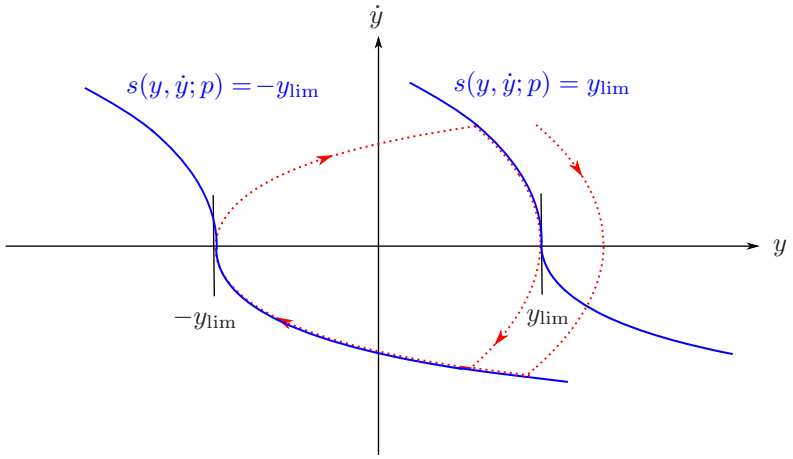

Figure 1: Switching curves (solid) and example of a trajectory (dotted) resulting from the application of the control scheme (22).

is a zero-mean periodic signal. By using (15)-(17), Problem 1 can be recast as that of finding a switching signal $v(t)$, guaranteeing that

$$|y(t)| \leq y_{\lim} \quad \text{for all } t \geq \bar{t} > 0, \tag{19}$$

where

$$0 < y_{\lim} \leq x_{\lim} - \max_t |\alpha(t)|. \tag{20}$$

Notice from (15) that the condition $k > p$ must be met, in order for the problem to be solvable. Moreover, by (20), one must have $x_{\lim} > \max_t |\alpha(t)|$, which is typically the case in real-world applications (since high-frequency disturbances $p_\Delta(t)$ are attenuated by the double integrator system (12)-(13)).

A minimum fuel and minimum switching solution to the above control problem is obtained by exploiting the results in [23]. Consider the switching function

$$s(y,\dot{y};p) = \begin{cases} y - \dfrac{1}{2(p-k)}\,\dot{y}^2 & \text{if} \quad \dot{y} \geq 0 \\ y - \dfrac{1}{2p}\,\dot{y}^2 & \text{if} \quad \dot{y} < 0. \end{cases} \tag{21}$$

Let the on/off input $v(t)$ be specified according to the hysteresis function

$$v(t) = \begin{cases} 1 & \text{if} \quad s(y(t),\dot{y}(t);p) \geq y_{\lim} \\ 0 & \text{if} \quad s(y(t),\dot{y}(t);p) \leq -y_{\lim} \\ v_h & \text{otherwise,} \end{cases} \tag{22}$$

where $v_h = 1$ if $s(y, \dot{y}; p) \geq y_{\lim}$ occurred more recently than $s(y, \dot{y}; p) \leq -y_{\lim}$, $v_h = 0$ otherwise. By applying the control law (22) to system (15), a limit cycle trajectory with amplitude $2y_{\lim}$ is reached in finite time from any initial condition. An example is shown in the phase plane portrait reported in Fig. 1. The limit cycle period is given by $T_L = 4\sqrt{\frac{k\, y_{\lim}}{p\, k - p^2}}$. It is divided into a firing period of length $T_F = DT_L$ and a coasting period of length $T_C = (1 - D)T_L$, where $D = p/k$ denotes the actuator duty cycle. Thus, the firing time turns out to be

$$T_F = \frac{4p}{k}\sqrt{\frac{k\, y_{\lim}}{p\, k - p^2}} = 4\sqrt{\frac{p\, y_{\lim}}{k^2 - k\, p}}. \tag{23}$$

4.2. RLS Filter Design

The control law (22) requires the real-time knowledge of $y(t)$, $\dot{y}(t)$ and p. Given the parameter p and the initial conditions $y(0)$, $\dot{y}(0)$, one can compute $y(t)$ and $\dot{y}(t)$ just by integrating system (15). However, using this solution would result in an open-loop control strategy. Moreover, the exact value of $y(0)$, $\dot{y}(0)$ and p is, in general, unknown.

An alternative approach consists in estimating $y(t)$, $\dot{y}(t)$ and p by using values of $x(t)$ obtained from inertial measurements. More specifically, the orbital elements $\gamma(t)$ and $\Omega(t)$ in (5) can be computed from absolute position and velocity measurements, by using standard analytical methods [16], while the quantities $\lambda_G(t)$, r and λ^* are known.

Let the obtained values of $x(t)$ be denoted as $\tilde{x}(t_j)$, where $\{t_j\}_{j\in\mathbb{N}}$ is the sequence of time samples at which measurements are taken. Now, observe that the solution to (15), with either $v = 0$ or $v = 1$, can be parameterized as

$$y(t) = \varphi^T(t)\theta, \tag{24}$$

where $\varphi(t) = [t^2\ t\ 1]^T$ and $\theta = [\theta_1\ \theta_2\ \theta_3]^T$ is a vector of unknown parameters to be determined. Hence, a least squares estimation problem can be cast as follows

$$\hat{\theta} = \arg\min_{\theta} \sum_j [\, \tilde{x}(t_j) - \varphi^T(t_j)\, \theta\,]^2. \tag{25}$$

A recursive solution to (25) is provided by the exponentially weighted RLS

algorithm [26]

$$\hat{\theta}(t_j) = \hat{\theta}(t_{j-1}) + \frac{P(t_{j-1})\,\varphi(t_j)}{\eta + \varphi(t_j)^T P(t_{j-1})\,\varphi^(t_j)} \left[\tilde{x}(t_j) - \varphi^T(t_j)\hat{\theta}(t_{j-1})\right] \quad (26)$$

$$P(t_j) = \frac{1}{\eta}\left[P(t_{j-1}) - \frac{P(t_{j-1})\,\varphi(t_j)\varphi^T(t_j)\,P(t_{j-1})}{\eta + \varphi^T(t_j)\,P(t_{j-1})\,\varphi(t_j)}\right], \quad (27)$$

initialized at $P(t_0)$ and $\hat{\theta}(t_0)$, where η is the forgetting factor.

The algorithm (26)-(27) is re-initialized each time that the right hand side of (15) changes sign, i.e., whenever the input switches, in order to prevent divergence in the estimates. Let $\bar{t}$ be an input switching time, such that $t_{s-1} < \bar{t} \leq t_s$. At time $\bar{t}$, the parameter vector is reset according to

$$\begin{aligned} \hat{\theta}_3(\bar{t}) &= \varphi^T(\bar{t})\,\hat{\theta}(t_{s-1}) \\ \hat{\theta}_2(\bar{t}) &= 2\,\hat{\theta}_1(t_{s-1})\,\bar{t} + \hat{\theta}_2(t_{s-1}) \\ \hat{\theta}_1(\bar{t}) &= \hat{\theta}_1(t_{s-1}) + k[v(t_{s-1}) - v(\bar{t})]/2. \end{aligned} \quad (28)$$

Then, (26)-(27) is applied by replacing $\varphi(t_j)$ with $\varphi(t_j - \bar{t})$, for $t_j \geq t_s$, and by setting the initial condition to $\hat{\theta}(\bar{t})$ given by (28). This ensures the continuity of $\varphi^T\hat{\theta}$ and of its first time derivative.

The continuous-time estimates of $y(t)$, $\dot{y}(t)$ and p returned by the filter are obtained by interpolation, as follows

$$\begin{aligned} \hat{y}(t) &= \varphi^T(t - \bar{t})\,\hat{\theta}(t_j) \\ \hat{\dot{y}}(t) &= 2(t - \bar{t})\,\hat{\theta}_1(t_j) + \hat{\theta}_2(t_j) \\ \hat{p}(t) &= 2\,\hat{\theta}_1(t_j) + k\,v(t), \end{aligned} \quad (29)$$

where t_j and $\bar{t}$ denotes the most recent measurement time and the most recent input switching time, respectively.

4.3. Adaptive Control Scheme Implementation

A real-time feedback control scheme is obtained by replacing $y(t)$, $\dot{y}(t)$ and p in (22), with the corresponding estimates $\hat{y}(t)$, $\hat{\dot{y}}(t)$ and $\hat{p}(t)$ provided by (29). The resulting adaptive control system is shown in Fig. 2.

It should now be remarked that the relationship (20) leaves some freedom in the choice of the control specification $y_{\lim}$. Such degree of freedom can be exploited to optimize other relevant performance criteria. Specifically, some applications require the satellite altitude to vary as little as possible, which

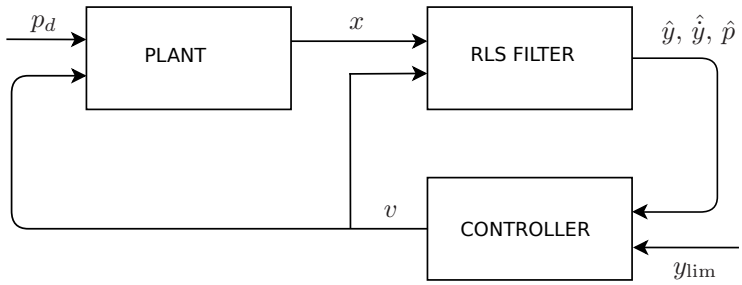

Figure 2: Block diagram of the closed-loop system.

corresponds to maintaining a near-zero orbital eccentricity. In this regard, atmospheric drag is know to have a stabilizing effect, as it tends to circularize the orbit. However, repeated groundtrack adjustment maneuvers can lead to a secular eccentricity growth. For nearly circular orbits, the variation in the orbital eccentricity due to the control acceleration u_T can be modeled as [19]

$$\dot{e} = 2\sqrt{\frac{a}{\mu}}\cos(f)\,u_T, \tag{30}$$

where e indicates the orbital eccentricity and f denotes the true anomaly. For small deviations about $a = a^*$, equation (30) can be approximated as

$$\dot{e} \approx 2\sqrt{\frac{a^*}{\mu}}\cos(n^*t + f_0)\,u_T, \tag{31}$$

where $n^* = \sqrt{\mu/(a^*)^3}$ is the reference mean motion.

The net change in e, $\Delta e = e(T) - e(0)$, obtained by applying a constant input $u_T = u_{\max}$ over a time interval of length T, can be computed from (31) according to

$$\Delta e = 2\,u_{\max}\sqrt{\frac{a^*}{\mu}}\int_0^T \cos(n^*t + f_0)\,\mathrm{d}t = \frac{2(a^*)^2 u_{\max}}{\mu}\Big[\sin(n^*T + f_0) - \sin(f_0)\Big]. \tag{32}$$

From (32) it follows that one possibility to enforce a zero secular growth $\Delta e = 0$ of the eccentricity is to set $T = T(m) = m\,\frac{2\pi}{n^*}$, i.e. to fire the engine for an integer multiple m of the orbital period. Another possibility is to initiate the maneuver at $f_0 = 0$ or $f_0 = \pi$ (assuming the periapsis exists) and set $T(m) = m\,\frac{\pi}{n^*}$, which amounts to firing for a multiple of half the orbital period (in particular, $T = \pi/n^*$ may be adopted to avoid firing the engine during eclipses). The corresponding y_{lim} can be found by equating $T(m)$ to the firing time T_F in (23),

thus resulting in

$$y_{\lim} = \frac{k(k-p)}{16\,p}\,T^2(m). \tag{33}$$

In order for the above strategy to be feasible, $y_{\lim}$ must satisfy condition (20). For typical values of $x_{\lim}$, k and p, this requirement can be met by adopting a sufficiently small value of m in (33). In this work, (33) is evaluated on-line, by using the disturbance estimate $\hat{p}$ returned by the RLS filter.

Finally, notice that the control law (21)-(22) by itself does not guarantee the firing sequence to be initiated at a specific true anomaly location f_0. In order to do so, once the condition $s(y, \dot{y}; p) \geq y_{\lim}$ is met, one has to postpone the engine activation $v = 1$ until f reaches f_0. The groundtrack error will grow only slightly during this time interval, since the true longitude dynamics are usually much faster than the error ones.

5. Simulation Case Study

An Earth observation mission performed by a 200 kg minisatellite equipped with EP has been simulated numerically, in order to validate the proposed approach. The spacecraft bus layout is modeled as a cube with side-length equal to 1 m. The truth model for the simulation consists of a numerical propagation routine based on Cowell's method, which accounts for the most relevant environmental perturbations affecting LEO satellites. Table 1 describes the main features of the simulation environment.

Table 1: Main features of the simulation model

Contribution	Model
Earth's Gravity	EGM96 9×9
Atmospheric Drag	NRLMSISE-00, $F_{10.7} = 220$, $A_p = 15$
Third Body	Luni-solar point mass gravity
Solar Pressure	Cannonball model with eclipses

The satellite is released in a near-circular sun-synchronous orbit with an altitude of about 460 km. The initial orbital elements, reported in Table 2, are chosen so as to achieve a repeat-groundtrack period of 3 days ($r = 3/46$ days/revs). Hence, the reference semi-major axis in (12) is $a^* = a(0)$. It is

Table 2: Initial conditions for the simulation

Orbital element	Initial value
Semi-major axis	$a(0) = 6838$ km
Eccentricity	$e(0) = 0.001$
Inclination	$i(0) = 97.28$ deg
RAAN	$\Omega(0) = 0$ deg
Argument of periapsis	$\omega(0) = 90$ deg
True anomaly	$f(0) = 270$ deg

required to keep groundtrack within a maximum deviation of 2 km from the nominal one at the equator, which corresponds to the error tolerance $x_{\text{lim}} = 2/R_{\oplus} = 3.136 \cdot 10^{-4}$ rad, where $R_{\oplus}$ denotes the Earth's equatorial radius. This level of accuracy is compatible with advanced scientific missions such as ICEsat [27].

The groundtrack control system relies on a GPS receiver providing position and velocity measurements, and on a low-power Hall Effect Thruster (HET). Table 3 reports the characteristics of the model used for the GPS and the HET. It is assumed that the thruster is aligned with the direction tangential to the orbit. The nominal acceleration provided by the HET amounts to $u_{\max} = F_{\max}/m_{\text{sat}} = 5 \cdot 10^{-5}$ m/s^2, where $F_{\max} = 0.01$ N and $m_{\text{sat}} = 200$ kg.

The measured values $\tilde{x}(t_j)$ of $x(t)$ are computed by first expressing GPS position and velocity measurements in terms of osculating orbital elements, and then transforming osculating elements into mean ones according to [28]. The forgetting factor of the RLS algorithm (26)-(27) is set to $\eta = 0.9999$. This provides a good trade-off between the sensitivity of the filter to high-frequency

Table 3: Characteristics of the control system

Device	Output	Std dev	Update time
GPS	Inertial position Inertial velocity	20 m 0.1 m/s	30 sec
HET	ON: 10 mN thrust OFF: no thrust	0.5 mN -	30 sec

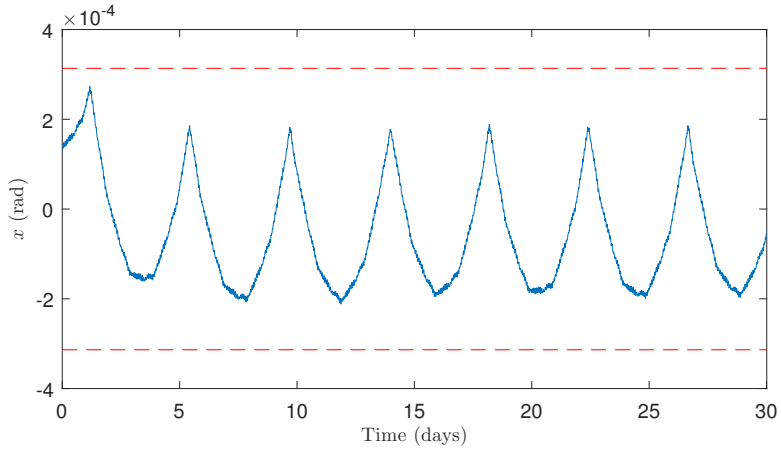

Figure 3: Tracking error $x(t)$ (solid) and error tolerance $\pm x_{\text{lim}}$ (dashed) .

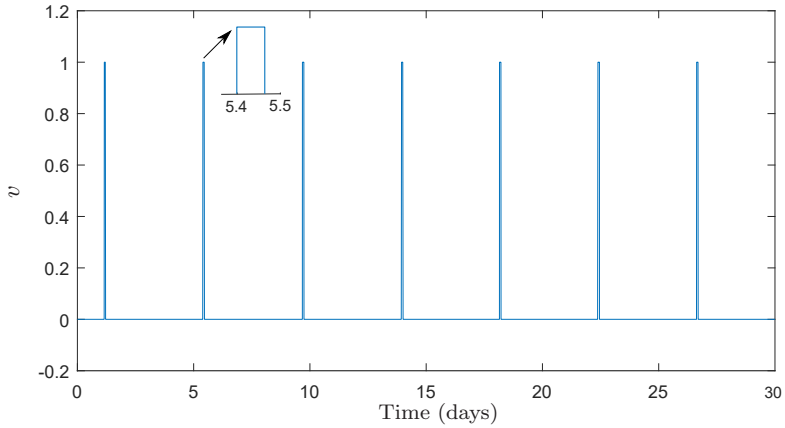

Figure 4: Switching command $v(t)$.

oscillations in $x(t)$ and its responsiveness to long-period drifts in $p_d(t)$ (e.g., due to seasonal changes in the atmospheric density), which are not modeled by (13). The error tolerance y_{lim} in (19) is set according to (33), with $T = T(m) = 2\pi/n^*$ and $p = \hat{p}$, resulting in $y_{\text{lim}} \simeq 2 \cdot 10^{-4}$ rad. This ensures that condition (20) is met with a good safety margin; at the same time, it allows one to successfully counteract the eccentricity variation in (32), according to the discussion in Section 4.3.

The mission is simulated for 30 days. The tracking error $x(t)$ resulting from the simulation is reported in Fig. 3. The corresponding switching command $v(t)$ is reported in Fig. 4. The controller is activated at $t \simeq 1$ day (after the RLS

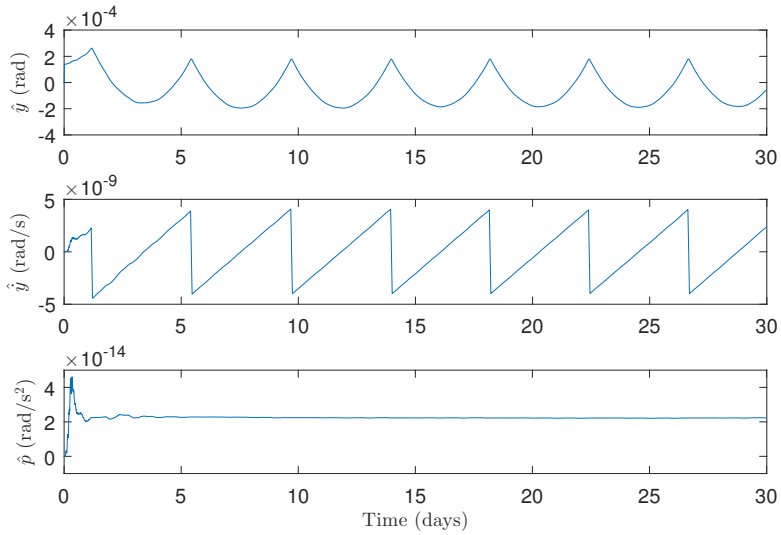

Figure 5: Estimates $\hat{y}(t)$, $\hat{\dot{y}}(t)$ and $\hat{p}(t)$ returned by the RLS filter.

filter transient has elapsed), in correspondence of the first peak in Fig 3. It can bee seen that a limit cycle with amplitude $2\,y_{\rm lim}$ is established from the second input transition onwards, and that the error is kept well within the maximum allowed deviation $x_{\rm lim}$ (represented by the dashed lines in Fig. 3). The HET engine is fired once about every 4 days, for a time interval of approximately 94 minutes. The duty cycle is equal to $D = 0.0156$: such a small value is due to the fact that the atmospheric drag force is much smaller than the 10 mN thrust force produced by the engine.

The signals $\hat{y}(t)$, $\hat{\dot{y}}(t)$ and $\hat{p}(t)$ estimated by the RLS filter are shown in Fig. 5. A zoom of the initial transient is depicted in Fig. 6, which reports also the average disturbance value p and the error signals $y(t)$, $\dot{y}(t)$ resulting from the solution of (15). It can be seen that the estimates converge in approximately one day. In particular, $\hat{p}(t)$ settles to a value which is very close to the average acceleration due to drag, as explained in Section 3. To better illustrate this fact, Figure 7 compares the estimated disturbance force $\hat{F} = m_{\rm sat}\, a^*\, \hat{p}(t)/(3\,r)$ with the absolute value $F_{\rm drag}$ of the drag force returned by the NRLMSISE-00 model, on the time interval $t \in [0, 36]$ hours. The oscillations in $F_{\rm drag}$ are due to changes in the atmospheric density induced by diurnal, latitudinal, and altitude variations. It is confirmed that the RLS filter is able to average out

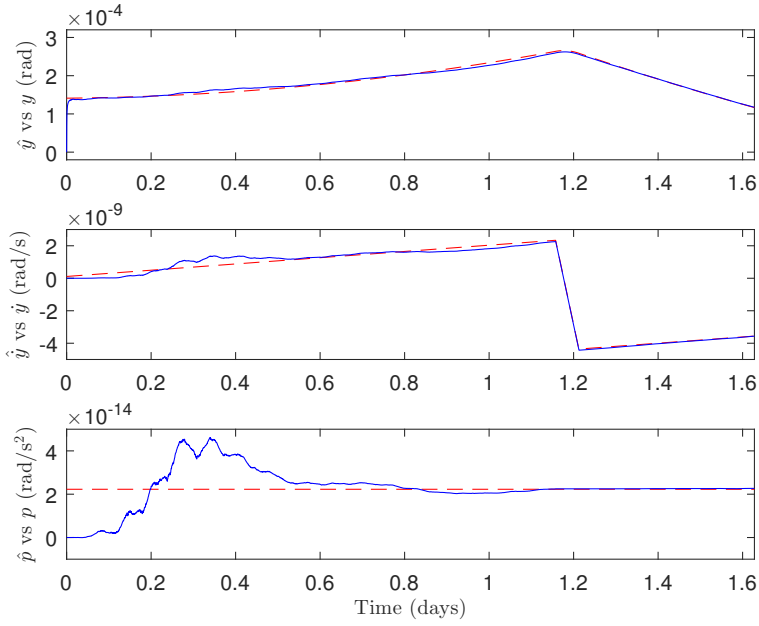

Figure 6: Estimates $\hat{y}(t)$, $\hat{\dot{y}}(t)$ and $\hat{p}(t)$ (solid) vs. reference signals $y(t)$, $\dot{y}(t)$ and $p(t)$ (dashed).

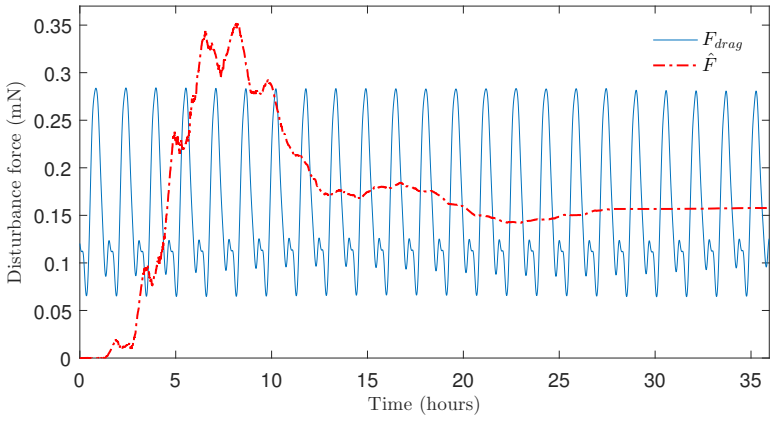

Figure 7: Profiles of F_{drag} (solid) and $\hat{F}$ (dash-dotted).

these effects, at steady-state. This is a key requirement for the implementation of the proposed control scheme.

The evolution of the orbital eccentricity is reported in Fig. 8. As expected, the proposed thrusting strategy has a negligible impact on this element, which shows a slow decrease due to environmental perturbations. Hence, the orbit of the spacecraft remains approximately circular during the entire simulation interval.

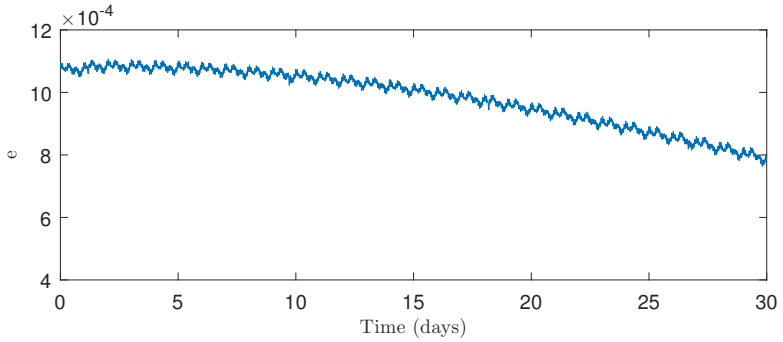

Figure 8: Evolution of the orbital eccentricity e.

Finally, the groundtrack profile resulting from the simulation has been compared to the uncontrolled one. As seen from Figs 9-10, the proposed method is able to compensate for the groundtrack drift due to perturbation effects, thus ensuring precise repeatability. It is worth stressing that the method requires neither a gravitational nor an atmospheric drag model: the controlled groundtrack automatically settles to the desired repeat condition, given only the parameter r in (5) and the measurements provided by the GPS. Moreover, notice that one may consider updating the parameter k in (16) on a periodic basis, should the engine acceleration deviate significantly from the nominal design value $u_{\max}$.

6. Conclusions

A simple and effective groundtrack maintenance strategy has been presented for low Earth orbiting satellites driven by low-thrust propulsion. The proposed adaptive control scheme consists of an hysteresis controller paired with a recursive least squares filter. It can be readily implemented within an autonomous guidance, navigation and control system. The results of a simulation case study show that the desired repeat-groundtrack pattern is acquired successfully and then maintained consistently by the control system. Such type of technology may play a key role in a number of future scientific and commercial space missions equipped with electric propulsion.

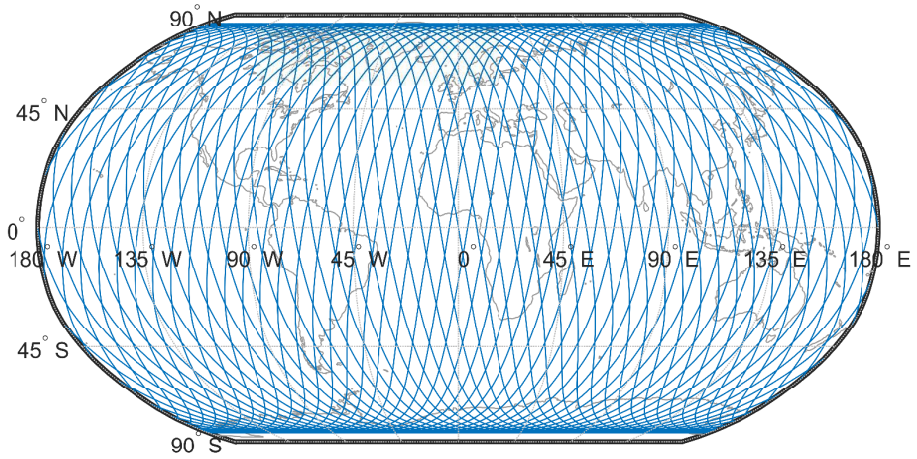

Figure 9: Controlled groundtrack.

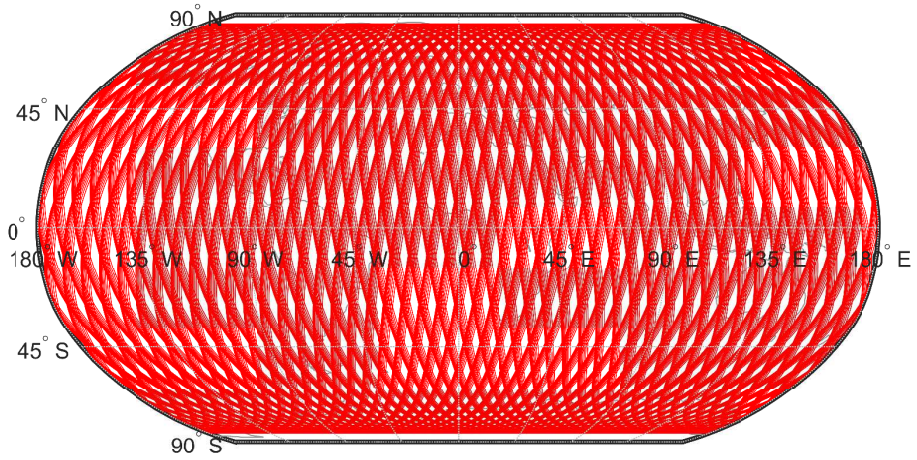

Figure 10: Uncontrolled groundtrack.

References

[1] A. Curiel, L. Boland, J. Cooksley, M. Bekhti, P. Stephens, W. Sun, M. Sweeting, First results from the disaster monitoring constellation (DMC), Acta Astronautica 56 (1–2) (2005) 261–271.

[2] G. Tyc, J. Tulip, D. Schulten, M. Krischke, M. Oxfort, The RapidEye mission design, Acta Astronautica 56 (1) (2005) 213–219.

[3] C. McLain, J. King, Future Ku-Band mobility satellites, in: 35th AIAA

International Communications Satellite Systems Conference, Trieste, Italy, 2017.

[4] D. Mortari, M. P. Wilkins, C. Bruccoleri, The flower constellations, Journal of Astronautical Sciences 52 (1) (2004) 107–127.

[5] M. Ruggieri, M. Sanctis, T. Rossi, M. Lucente, D. Mortari, C. Bruccoleri, P. Salvini, V. Nicolai, The flower constellation set and its possible applications, Tech. rep., Advanced Concept Team, ESA (2006).

[6] J. R. Wertz, J. T. Collins, S. Dawson, H. J. Koenigsmann, C. W. Potterveld, Autonomous constellation maintenance, in: Mission Design & Implementation of Satellite Constellations, 1998, pp. 263–273.

[7] A. Garulli, A. Giannitrapani, M. Leomanni, F. Scortecci, Autonomous low-Earth-orbit station-keeping with electric propulsion, Journal of Guidance, Control, and Dynamics 34 (6) (2011) 1683–1693.

[8] S. De Florio, S. D'Amico, G. Radice, Virtual formation method for precise autonomous absolute orbit control, Journal of Guidance, Control, and Dynamics 37 (2) (2014) 425–438.

[9] A. Weiss, U. V. Kalabić, S. Di Cairano, Station keeping and momentum management of low-thrust satellites using MPC, Aerospace Science and Technology 76 (2018) 229–241.

[10] IADC space debris mitigation guidelines, Inter-Agency Space Debris Coordination Committee, 2007, revision 1.

[11] M. Guelman, A. Kogan, Electric propulsion for remote sensing from low orbits, Journal of Guidance, Control, and Dynamics 22 (2) (1999) 313–321.

[12] D. G. Fearn, Economical remote sensing from a low altitude with continuous drag compensation, Acta Astronautica 56 (5) (2005) 555–572.

[13] W. Wright, P. Ferrer, Electric micropropulsion systems, Progress in Aerospace Sciences 74 (2015) 48 – 61.

[14] M. Leomanni, A. Garulli, A. Giannitrapani, F. Scortecci, Propulsion options for very low Earth orbit microsatellites, Acta Astronautica 133 (2017) 444–454.

[15] D. Lev, R. M. Myers, K. M. Lemmer, J. Kolbeck, M. Keidar, H. Koizumi, H. Liang, D. Yu, T. Schönherr, J. G. del Amo, et al., The technological and commercial expansion of electric propulsion in the past 24 years, in: 35th International Electric Propulsion Conference, Atlanta, US, 2017.

[16] D. A. Vallado, Fundamental of Astrodynamics and Applications, 2nd Edition, Microcosm Press, El Segundo, California, 2001.

[17] M. Aorpimai, P. Palmer, Repeat-groundtrack orbit acquisition and maintenance for Earth-observation satellites, Journal of guidance, control, and dynamics 30 (3) (2007) 654–659.

[18] P. Sengupta, S. R. Vadali, K. T. Alfriend, Satellite orbit design and maintenance for terrestrial coverage, Journal of Spacecraft and Rockets 47 (1) (2010) 177–187.

[19] X. Fu, M. Wu, Y. Tang, Design and maintenance of low-Earth repeat-ground-track successive-coverage orbits, Journal of Guidance, Control, and Dynamics 35 (2) (2012) 686–691.

[20] Y. He, M. Xu, X. Jia, R. Armellin, High-precision repeat-groundtrack orbit design and maintenance for Earth observation missions, Celestial Mechanics and Dynamical Astronomy 128 (2-3) (2017) 275–294.

[21] G. Zhang, X. Cao, Coplanar ground-track adjustment using time difference, Aerospace Science and Technology 48 (2016) 21–27.

[22] G. Di Mauro, R. Bevilacqua, D. Spiller, J. Sullivan, S. D'Amico, Continuous maneuvers for spacecraft formation flying reconfiguration using relative orbit elements, Acta Astronautica 153 (2018) 311–326.

[23] A. Garulli, A. Giannitrapani, M. Leomanni, Minimum switching control for systems of coupled double integrators, Automatica 60 (2015) 115–121.

[24] M. Leomanni, A. Garulli, A. Giannitrapani, F. Farina, F. Scortecci, Minimum switching thruster control for spacecraft precision pointing, IEEE Transactions on Aerospace and Electronic Systems 53 (2) (2017) 683–697.

[25] S. D'Amico, O. Montenbruck, Proximity operations of formation-flying spacecraft using an eccentricity/inclination vector separation, Journal of Guidance Control and Dynamics 29 (3) (2006) 554–563.

[26] L. Ljung, System identification - theory for the user, Prentice-Hall, Englewood Cliff, N.J., 1987.

[27] B. Schutz, H. Zwally, C. Shuman, D. Hancock, J. Di Marzio, Overview of the ICESat mission, Geophysical Research Letters 32 (21) (2005) .

[28] D. Brouwer, Solution of the problem of artificial satellite theory without drag, The Astronomical Journal 64 (1959) 378–397.